COBEM 2023 27TH INTERNATIONAL CONGRESS OF MECHANICAL ENGINEERING

ABCM Brazilian Society of Mechanical Sciences and Engineering
27th ABCM International Congress of Mechanical Engineering
December 04-08, 2023, Florianópolis-SC, Brazil

COB-2023-1663
NOVEL IMPLEMENTATION OF ASYMPTOTIC HOMOGENIZATION (NIAH) APPLIED TO FRAME-LIKE PERIODIC MATERIALS

Augusto Henrique dos Santos
Pablo Andrés Muñoz Rojas
Departamento de Engenharia Mecânica
Universidade do Estado de Santa Catarina, Brasil
e-mails augusto_hssantos@hotmail.com, pablo.munoz@udesc.br

Abstract. *Technological breakthroughs increasingly demand materials capable of meeting multifunctional requirements. Frame-Like Periodic Cellular Materials (FLPM), have gained prominence in this scenario especially since innovations as additive manufacture allow their fabrication even for complex base cells. As cellular metamaterials display heterogeneous properties within a typical cell, the prediction of their macroscopic behavior can be addressed using asymptotic homogenization (AH) coupled to the Finite Element Method (FEM). Aiming at computational efficiency, the base cell discretization is often performed using bar elements, although the use of frame elements would be more reliable because moments and torque are transmitted. In this work we use the "novel implementation of the asymptotic homogenization (NIAH)" to obtain the homogenized elasticity tensors for FLPMs based on Euler-Bernoulli frame elements. A new step is introduced in the original version of NIAH to account for the rotational degrees of freedom. We compare the results given by this modified NIAH with analytical solutions for specific topologies of FLPM available in literature. It is observed that the accuracy of homogenized properties strongly depends on the layout of the base cell employed. Hence, we propose a systematic procedure to define the geometry of the base cell in order to obtain enhanced results.*

Keywords: *Asymptotic homogenization, NIAH, Frame-like periodic cellular materials, Euler-Bernoulli beams*

1. INTRODUCTION

Periodic materials are described by the repetition of their base cells, which possess much smaller dimensions than the dimensions of the global domain. The determination of the effective properties of such materials can be done by analyzing a single unit cell (Hassani and Hinton, 1998). Figure 1 displays some frame-like periodic materials and their periodic unit cells (Weeks, 2022)

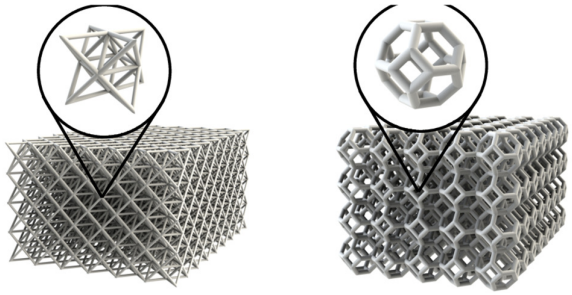

Figure 1 –Frame-like periodic materials and respective base cells (Weeks, 2022): (a) octet-truss and (b) Kelvin topologies.

Periodicity means that all the physical charecteristics such as, mechanical and thermal ones must obey the relation

$$\mathcal{F}(\boldsymbol{x} + \boldsymbol{NY}) = \mathcal{F}(\boldsymbol{x}), \tag{1}$$

where $\mathcal{F}$ is a scalar, vector or tensor physical property, $\boldsymbol{x} = [x_1, x_2, x_3]^T$ is the position vector of an arbitrary point, $\boldsymbol{N}$ is a diagonal integer 3 x 3 matrix with components n_1, n_2 and n_3, which are responsible for the translation of the cell in the 3 principal directions, that is

$$\boldsymbol{N} = \begin{bmatrix} n_1 & 0 & 0 \\ 0 & n_2 & 0 \\ 0 & 0 & n_3 \end{bmatrix}, \tag{2}$$

and, finally, $\boldsymbol{Y} = [Y_1, Y_2, Y_3]^{\boldsymbol{T}}$ is a constant vector that determines the period of the structure, i.e., the dimensions of the base cell. In homogenization theory, the period is considered to be much smaller than the dimension of the global domain.

We consider that the material can be divided into two scales, the macroscale $\boldsymbol{x}$ and the microscale $\boldsymbol{y}$, and that the ratio between the real lengths of unit vectors of such scales is given by

$$\boldsymbol{y} = \frac{1}{\epsilon}\boldsymbol{x}, \tag{3}$$

where ϵ is a very small parameter, such that the value of $\frac{1}{\epsilon}$ (or magnification parameter) represents the magnitude of the expansion necessary to make the dimension of the base cell comparable to the dimension of the material (Hassani and Hinton, 1998).

In Fig. 2, a unit cell is composed of 8 bars, connecting 5 nodes. Each bar has its own Young modulus and cross section area, and the rest of the cell domain is void, so at this scale the domain is clearly heterogeneous. Asymptotic homogenization allows to model the average material behavior of the cell, so that the heterogeneous behavior is replaced by the homogenized elastic tensor $\boldsymbol{E}^H$, which is replaced at the macroscopic point P

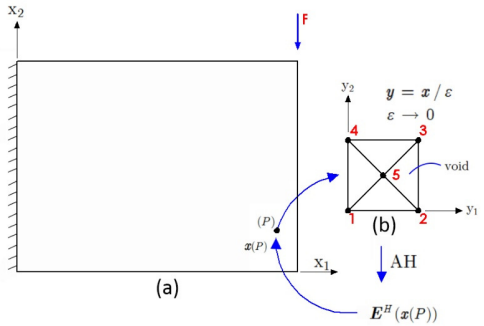

Figure 2 – Homogenized elastic tensor $\boldsymbol{E}^H$ (Jagiello and Muñoz-Rojas, 2021): (a) a continuum domain modeled by asymptotic homogeneization ; (b) the unit cell is composed of a truss-like structure..

2. HOMOGENEIZATION OF ELASTIC PROPERTIES

We start with the asymptotic expansion of the displacement field into two scales, the macroscopic scale $\boldsymbol{u_0(x)}$ and the microscopic scale $\boldsymbol{u_1(x)}$:

$$\boldsymbol{u(x,y)} = \boldsymbol{u_0(x)} + \epsilon \boldsymbol{u_1(x,y)}, \tag{4}$$

where $\boldsymbol{u_1}$ is periodic in the dimension Y of the cell and the lower indices "0" and "1" correspond to the macro and microscales, respectively.

Considering that there are no traction efforts acting on the internal borders of the base cell, the principle of virtual work can be stated as

$$\int_\Omega \boldsymbol{\sigma}: \boldsymbol{\delta\varepsilon} d\Omega - \int_\Omega \boldsymbol{b}.\boldsymbol{\delta u} d\Omega - \int_\Gamma \boldsymbol{t}.\boldsymbol{\delta u} d\Gamma = 0 \quad \forall\, \boldsymbol{\delta u} \in V_\Omega, \tag{5}$$

where $\boldsymbol{\sigma}$ is the stress, $\boldsymbol{\varepsilon}$ is the strain, $\boldsymbol{b}$ is the body force, $\boldsymbol{t}$ is the surface force acting on the boundary Γ, $\boldsymbol{\delta u}$ is the virtual displacement suffered by the structure and V_Ω is the set of kinematically admissible displacements.

Defining the operator

$$\partial_{\boldsymbol{x}} = \frac{1}{2}\left(\frac{\partial(.)_k}{\partial x_l} + \frac{\partial(.)_l}{\partial x_k}\right), \tag{6}$$

after some algebra, we obtain the macroscopic equation (Muñoz-Rojas et al, 2010) as

$$\int_\Omega \partial_{\boldsymbol{x}} \boldsymbol{\delta u_0}: \boldsymbol{E^H}: \partial_{\boldsymbol{x}} \boldsymbol{u_0} d\Omega - \int_\Omega \langle \boldsymbol{b} \rangle . \boldsymbol{\delta u_0} d\Omega - \int_\Gamma \boldsymbol{t} \cdot \boldsymbol{\delta u_0} d\Gamma = 0, \tag{7}$$

where $\langle \boldsymbol{b} \rangle$ is the average of the body force on the cell and $\boldsymbol{E^H}$ is the homogenized constitutive elastic tensor, given by

$$\boldsymbol{E^H} = \frac{1}{|\boldsymbol{Y}|}\int_{\boldsymbol{Y}} \boldsymbol{E} : \left(\boldsymbol{I} - \partial_y \boldsymbol{\chi}\right) dY. \tag{8}$$

Equation (8) can be expressed in component form as

$$E^H_{ijkl}(\boldsymbol{x}) = \frac{1}{|\boldsymbol{Y}|}\int_{\boldsymbol{Y}} \left(E_{ijkl} - E_{ijkl}\frac{\partial \chi^{kl}_p}{\partial y_q}\right) dY. \tag{9}$$

where χ^{kl}_p is the set of characteristic displacements obtained by solving the microscopic equation

$$\int_Y \partial_{\boldsymbol{y}} \boldsymbol{\delta u_1} : \boldsymbol{E} : \partial_{\boldsymbol{y}} \boldsymbol{\chi} dY = \int_Y \partial_{\boldsymbol{y}} \boldsymbol{\delta u_1} : \boldsymbol{E} : \boldsymbol{I} dY, \tag{10}$$

in which $\boldsymbol{I}$ is the 4th order identity tensor.

Further details can be found in Guedes and Kikuchi (1990), Hassani and Hinton (1998) and Muñoz-Rojas et al. (2010)

3. TRADITIONAL IMPLEMENTATION OF ASYMPTOTIC HOMOGENIZATION

In order to obtain the characteristic displacements $\boldsymbol{\chi}$ of Eqs. (8-9), Eq. (10) is solved using the finite element method on the domain of the unit frame-like base cell. Using Voigt compact notation, a numerical approximation of $\boldsymbol{\chi}$ can be obtained using linear 3D bar or frame finite elements (Yan et al., 2006). The resulting discretized problem is

$$\boldsymbol{K\chi} = \boldsymbol{P}, \tag{11}$$

or

$$[\boldsymbol{K}]\left[\boldsymbol{\chi^{(11)}}, \boldsymbol{\chi^{(22)}}, \boldsymbol{\chi^{(33)}}, \boldsymbol{\chi^{(12)}}, \boldsymbol{\chi^{(23)}}, \boldsymbol{\chi^{(13)}}\right] = \left[\left[\boldsymbol{P^{(11)}}, \boldsymbol{P^{(22)}}, \boldsymbol{P^{(33)}}, \boldsymbol{P^{(12)}}, \boldsymbol{P^{(23)}}, \boldsymbol{P^{(13)}}\right]\right], \tag{12}$$

where

$$\boldsymbol{K} = \bigcup_{\boldsymbol{e=1}}^{\boldsymbol{nel}} \int_{\Omega^e} \boldsymbol{B}^T \boldsymbol{D} \boldsymbol{B} \boldsymbol{d} Y^e, \tag{13}$$

$$\boldsymbol{P} = \bigcup_{\boldsymbol{e=1}}^{\boldsymbol{nel}} \int_{\Omega^e} \boldsymbol{B}^T \boldsymbol{D} \boldsymbol{I} \boldsymbol{d} Y^e \tag{14}$$

In these equations, $\boldsymbol{K}$ is the global stiffness matrix, $\boldsymbol{P}$ is the matrix containing, in each column, one of the global load cases that arise in the homogenization formulation (the columns of $\boldsymbol{I}$ in Eq. (10)), $\boldsymbol{B}$ is the strain-displacement matrix, $\boldsymbol{D}$ is the local 1-D constitutive matrix of the bar element rotated to the global system of reference, Ω^e is the element domain and Y^e is the volume of the element. For solving the system of Eq. (11) we adopt periodic boundary conditions.

3.1 Periodic boundary conditions

The boundary conditions used come from the periodicity of the unit cells assumed in the homogenization formulation. Hence, the displacement field must show the same values on opposite sides of the cell (not necessarily a square cell, as will be seen afterwards). We impose such equality using the condensation method (Yang and Becker, 2004). One of the cell vertices is constrained not to move and a Boolean transformation matrix $\boldsymbol{T}$ is defined relating all the degrees of freedom $\boldsymbol{\chi}$ to a vector containing the independent (master) degrees of freedom $\widetilde{\boldsymbol{\chi}}$. The relation can be expressed as

$$\boldsymbol{\chi} = \boldsymbol{T}\widetilde{\boldsymbol{\chi}}. \tag{15}$$

In this way, the global system of equations is replaced by the reduced system

$$\widetilde{\boldsymbol{K}}\widetilde{\boldsymbol{\chi}} = \widetilde{\boldsymbol{P}}, \tag{16}$$

where

$$\widetilde{\boldsymbol{K}} = \boldsymbol{T^T K T} \tag{17}$$

and

$$\widetilde{\boldsymbol{P}} = \boldsymbol{T^T P}. \tag{18}$$

Further details can be seen in Jagiello and Muñoz-Rojas (2021). Notice that periodic boundary conditions can also be imposed by simple multipoint constraints, Lagrange multipliers, among other methods.

4. NEW IMPLEMENTATION OF ASYMPTOTIC HOMOGENIZATION (NIAH)

The new implementation of asymptotic homogenization (Cheng, Cai and Xu, 2013) starts from Eq. (14) of the traditional asymptotic homogenization (AH), but is rewritten so that the imposed unit strain fields $\boldsymbol{\varepsilon^0}$ can be replaced by an equivalent displacement field $\boldsymbol{\chi^0}$, such that

$$\boldsymbol{P} = \int_Y \boldsymbol{B}^T \boldsymbol{D}\boldsymbol{\varepsilon}^0 dY = \int_Y \boldsymbol{B}^T \boldsymbol{D}\boldsymbol{B} dY \cdot \boldsymbol{\chi}^0 = \boldsymbol{K}\boldsymbol{\chi}^0. \tag{19}$$

It can be seen that each load vector composing the global matrix $\boldsymbol{P}$ can be obtained directly by the product of the stiffness matrix $\boldsymbol{K}$ by the respective vector of the displacement field $\boldsymbol{\chi^0}$.

Taking as an example the 3D case, the displacement field to be employed is

$$\boldsymbol{\chi_{node}} = [u, v, w]^{\boldsymbol{T}},$$

$$\boldsymbol{\chi^0_{node}} = \left[\boldsymbol{\chi^{0(11)}}, \boldsymbol{\chi^{0(22)}}, \boldsymbol{\chi^{0(33)}}, \boldsymbol{\chi^{0(12)}}, \boldsymbol{\chi^{0(23)}}, \boldsymbol{\chi^{0(13)}}\right], \tag{20}$$

$$\boldsymbol{\chi^0_{node}} = \begin{bmatrix} x & 0 & 0 & 0.5y & 0 & 0.5z \\ 0 & y & 0 & 0.5x & 0.5z & 0 \\ 0 & 0 & z & 0 & 0.5y & 0.5x \end{bmatrix},$$

where $\boldsymbol{\chi^{0(kl)}_{node}}$ represents a fragment of the vector of displacements equivalent to the unit strains for each load case, relative to a given node where x, y and z are the nodal coordinates in the global system of reference.

It is important to remark that the periodic boundary conditions are not imposed at this stage and that the prescribed displacements equivalent to the unit strain fields must be applied to all the nodes.

Once the vectors of nodal loads that compose $\boldsymbol{P}$ are obtained, these are used to solve Eq. (11), this time enforcing the periodic boundary conditions. The characteristic displacements $\boldsymbol{\chi}^{*(kl)}$ are, therefore, determined (corresponding to the same field $\boldsymbol{\chi}^{(kl)}$ that would be obtained using the traditional asymptotic homogenization (AH). The asterisk is used only to distinguish traditional AH and NIAH). Thereafter, the characteristic displacements $\boldsymbol{\chi}^{*(kl)}$ are imposed as prescribed displacements in order to find the vector force $\boldsymbol{P}^{*(kl)}$, which is given by

$$\boldsymbol{P}^{*(kl)} = \boldsymbol{K}\boldsymbol{\chi}^{*(kl)}. \tag{21}$$

Finally, the homogenized constitutive elastic tensor can be obtained using Eq. (9) rewritten in terms of the strain energy (Sigmund, 1994),

$$E^H_{ijkl} = \frac{1}{|Y|}\int_Y E_{pqrs}\left(\varepsilon^{0(ij)}_{pq} - \varepsilon^{*(ij)}_{pq}\right)\left(\varepsilon^{0(kl)}_{rs} - \varepsilon^{*(kl)}_{rs}\right)dY, \tag{22}$$

or, in matrix notation,

$$E^H_{ijkl} = \frac{1}{|Y|}\int_Y (\boldsymbol{\varepsilon^{0}}^{(ij)} - \boldsymbol{\varepsilon}^{*(ij)})^T \boldsymbol{E}\,(\boldsymbol{\varepsilon}^{0(kl)} - \boldsymbol{\varepsilon}^{*(kl)})dY, \tag{23}$$

$$E^H_{ijkl} = \frac{1}{|Y|}(\boldsymbol{\chi}^{0(ij)} - \boldsymbol{\chi}^{*(ij)})^T \boldsymbol{K}(\boldsymbol{\chi}^{0(kl)} - \boldsymbol{\chi}^{*(kl)}). \tag{24}$$

Replacing Eqs. (19) and (21) in Eq. (24) yields the expression for the homogenized constitutive elastic tensor, as follows

$$E^H_{ijkl} = \frac{1}{|Y|}(\boldsymbol{\chi}^{0(ij)} - \boldsymbol{\chi}^{*(ij)})^T(\boldsymbol{P}^{(kl)} - \boldsymbol{P}^{*(kl)}). \tag{25}$$

4.1 Consideration of rotations in the Euler-Bernoulli beams using NIAH

It is clear that the NIAH procedure evaluates the macroscopic strain field based on the values of nodal translations within the base cell, as exemplified in Eq. (20). This allows straightforward use of bar elements in the microscale, since they only have translational degrees of freedom. However, in the case of frames, we must take into consideration nodal

rotations in addition to displacements. To this end, we propose an additional step in the original NIAH procedure. We impose the prescribed translational displacements given in Eq. (20) and solve the system

$$\boldsymbol{K\chi^0 = 0}, \tag{26}$$

where the rotations are unknown. Once the displacement field $\boldsymbol{\chi^0}$ is completely determined, with known values for the nodal rotations, it is possible to calculate the loading vectors $\boldsymbol{P}^{(kl)}$, using Eq. (19). Thereafter, application of Eq. (11) is straightforward, and the characteristic displacements $\boldsymbol{\chi}^{*(kl)}$ are obtained. Finally, the constitutive elastic tensor can be calculated using Eq. (25). Figure 3 summarizes the steps of the NIAH adapted to the frame-like unit cells.

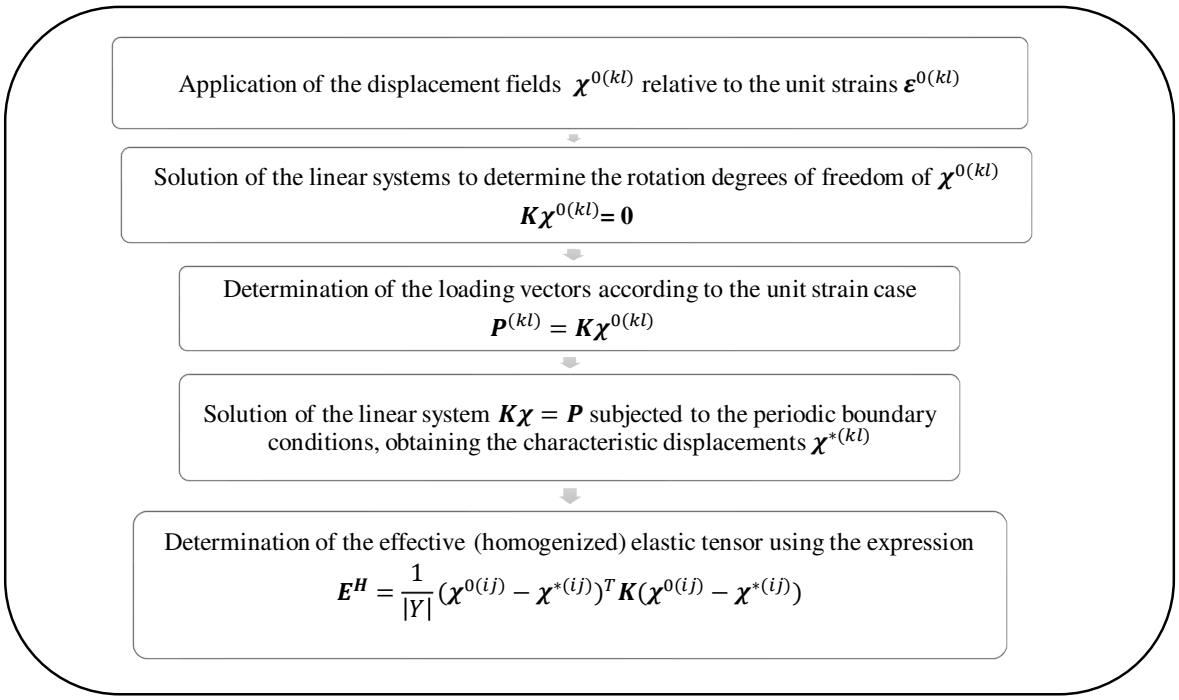

Figure 3. Algorithm for the new implementation of asymptotic homogenization (NIAH) adapted to Euler- Bernoulli frame elements.

5. NUMERICAL RESULTS

Using an object-oriented symbolic algebra algorithm and homogenization based on the equivalent strain energy, Sam *et al.* (2017) provide analytical expressions for some elastic constitutive parameters of periodic materials made of frame-like base cells. In this Section, we use some of their expressions for 2D and 3D given base cells, to compare to the results of our proposed procedure. In the 2D examples, we adopt unit values for Young modulus E and for the dimension L of the square base cell. The cross section of the frames is square with width w and moment of inertia I. The volume of the 2D cell is $V_C = wL^2$. We present results for $w = 0.1$ and $w = 0.2$ units of normalized length.

5.1 2D Body-centered square

The *body-centered square* cell is classified as being *stretching-dominated*. This means that although its elements bend, they suffer predominantly axial strains when subjected to external loading. Figure 4 (a) displays representative region of a structure of the type *body-centered square*. Three different configurations, named I, II and III, are selected as base cells for the evaluation of effective elastic properties of the material. All the cell configurations have the same volume and relative density. For this structure, Sam *et al.* (2017) use the base cell with configuration II.

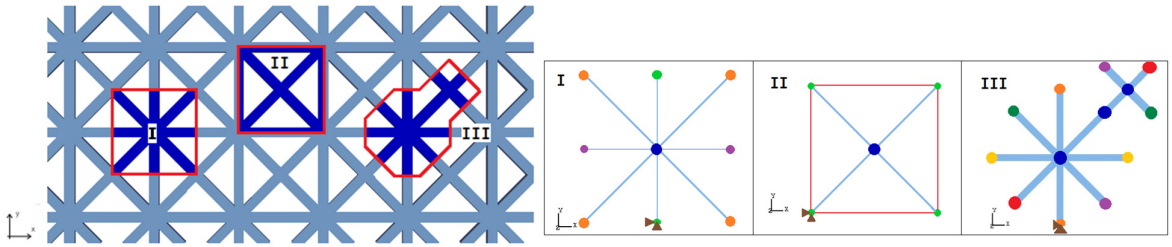

(a) (b)

Figure 4. (a) Body-centered square with three different configurations for the base cell, (b) Detail for describing data information for each type of base cell.

Figure 4 (b) shows how boundary conditions and properties of the element cross sections are input in the second stage of NIAH, for each configuration. Nodes with the same color share the same boundary conditions due to periodicity, blue nodes are internal nodes, light blue elements have cross sections A e moments of inertia I, while red elements have cross sections $A/2$ e moments of inertia $I/2$. Brown triangles stand for displacement constraints.

Table 1 displays the elastic constitutive tensors obtained for each of the configurations using the procedure proposed in this work. Table 2 and 3 compare the corresponding values of E, G and ν with the analytical values given by Sam *et al.* (2017). The expressions the analytical results taken as reference are given in Eq. (27)

Table 1. Homogenized elastic tensors for configurations I, II and III of body-centered square base cells.

Base cell configuration	$\boldsymbol{E^H}(w = 0.1)$	$\boldsymbol{E^H}(w = 0.2)$
I	$\begin{bmatrix} 0.17106 & 0.07036 & 0 \\ 0.07036 & 0.17106 & 0 \\ 0 & 0 & 0.07121 \end{bmatrix}$	$\begin{bmatrix} 0.34425 & 0.13859 & 0 \\ 0.13859 & 0.34425 & 0 \\ 0 & 0 & 0.14542 \end{bmatrix}$
II	$\begin{bmatrix} 0.17134 & 0.07008 & 0 \\ 0.07008 & 0.17134 & 0 \\ 0 & 0 & 0.07121 \end{bmatrix}$	$\begin{bmatrix} 0.34647 & 0.13638 & 0 \\ 0.13638 & 0.34647 & 0 \\ 0 & 0 & 0.14542 \end{bmatrix}$
III	$\begin{bmatrix} 0.17212 & 0.06929 & 0 \\ 0.06929 & 0.17212 & 0 \\ 0 & 0 & 0.07121 \end{bmatrix}$	$\begin{bmatrix} 0.35274 & 0.13011 & 0 \\ 0.13011 & 0.35274 & 0 \\ 0 & 0 & 0.14542 \end{bmatrix}$

Table 2. Comparison of constitutive parameters obtained in this work (NIAH) with the analytical values given by Sam et al. (2017) for the body-centered square structure with $w = 0.1$.

Constitutive parameter w = 0.1	NIAH Configuration I	NIAH Configuration II	NIAH Configuration III	Analytical Sam *et al.* (2017)
E^*	1.421×10^{-1}	1.427×10^{-1}	1.442×10^{-1}	1.442×10^{-1}
G^*	7.121×10^{-2}	7.121×10^{-2}	7.121×10^{-2}	7.121×10^{-2}
υ^*	4.113×10^{-1}	4.090×10^{-1}	4.026×10^{-1}	4.026×10^{-1}

Table 3. Comparison of constitutive parameters obtained in this work (NIAH) with the analytical values given by Sam et al. (2017) for the body-centered square structure with $w = 0.2$.

Constitutive parameter w = 0.2	NIAH Configuration I	NIAH Configuration II	NIAH Configuration III	Analytical Sam *et al.* (2017)
E^*	2.884×10^{-1}	2.928×10^{-1}	3.047×10^{-1}	3.047×10^{-1}
G^*	1.454×10^{-1}	1.454×10^{-1}	1.454×10^{-1}	1.454×10^{-1}
υ^*	4.026×10^{-1}	3.936×10^{-1}	3.689×10^{-1}	3.689×10^{-1}

The reference analytical expressions for the 2D body centered square cell are (Sam *et al.,* 2017)

$$E^* = \frac{E}{V_C}\left[\frac{\sqrt{2}(AL)^2+48(AI)}{(AL)+\left(\frac{24\sqrt{2}}{2+\sqrt{2}}\right)\left(\frac{I}{L}\right)}\right], \tag{27}$$

$$G^* = \frac{E}{V_C}\left[\left(\frac{\sqrt{2}}{2}\right)(AL) + 6\left(\frac{I}{L}\right)\right] \tag{28}$$

$$\upsilon^* = \frac{\left(\frac{\sqrt{2}}{2+\sqrt{2}}\right)(AL)-\left(\frac{24\sqrt{2}}{2+\sqrt{2}}\right)\left(\frac{I}{L}\right)}{(AL)+\left(\frac{24\sqrt{2}}{2+\sqrt{2}}\right)\left(\frac{I}{L}\right)}. \tag{29}$$

Notice that although the constitutive parameters obtained using NIAH for each configuration can be considered close, they do not match exactly. Only the shear modulus is identical for all the cases, indicating that all the configurations respond identically to the third load case, which corresponds to the strain field given by $\boldsymbol{\varepsilon^0} = [0, 0, 1]$. However, it is remarkable that the base cell with configuration III coincides with the values given by Sam *et al.* (2017) for all the constitutive parameters. It is of utmost importance to observe that different from configurations I and II, the borders of the base cell with configuration III cuts the frame elements only perpendicularly to their axes.

Another interesting issue is that for configurations I and II, the difference between NIAH and the analytical results increases for increasing values of w.

We use these findings to evaluate the application of the proposed procedure to a 3D problem.

5.2 3D Body-centered cubic

The *body-centered cubic* cell is the 3D extension of the 2D *body-centered square* cell. Hence, it shows symmetry with respect to the axes directions. Figure 5 displays the isometric and topografic views for a *body-centered cubic* cell. Different from the 2D case, here the bars have a circular cross section defined by their diameter *D*.

Isometric view	Topografic view
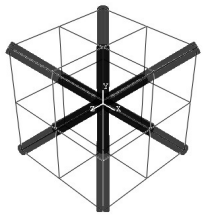	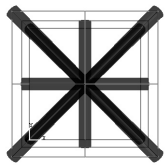

Figure 5. Different views for the body-centered cubic cell.

For this cell, the adapted NIAH procedure proposed in this work provides the elastic constitutive tensors shown in Table 4. The validation is performed by comparison of the corresponding constitutive parameters with the ones given by Sam et al. (2017), according to Table 5.

Table 4. Homogenized elastic tensors for the simple cubic base cell for different cross section diameters.

$\boldsymbol{E^H}(D = 0.1)$	$\begin{bmatrix} 0.013946 & 0.006023 & 0.006023 & 0 & 0 & 0 \\ & 0.007854 & 0.006023 & 0 & 0 & 0 \\ & & 0.007854 & 0 & 0 & 0 \\ & & & 0.006091 & 0 & 0 \\ & sym & & & 0.006091 & 0 \\ & & & & & 0.006091 \end{bmatrix}$
$\boldsymbol{E^H}(D = 0.2)$	$\begin{bmatrix} 0.056342 & 0.023813 & 0.023813 & 0 & 0 & 0 \\ & 0.056342 & 0.023813 & 0 & 0 & 0 \\ & & 0.056342 & 0 & 0 & 0 \\ & & & 0.024903 & 0 & 0 \\ & sym & & & 0.024903 & 0 \\ & & & & & 0.024903 \end{bmatrix}$

Table 5. Comparison of constitutive parameters obtained in this work (NIAH) with the analytical values given by Sam et al. (2017) for the body-centered cubic structure with $D = 0.1$ and $D = 0.2$.

Constitutive parameter	NIAH $D = 0.1$	Sam et al. (2017) $D = 0.1$	NIAH $D = 0.2$	Sam et al. (2017) $D = 0.2$
E^*	1.031×10^{-2}	1.044×10^{-2}	4.219×10^{-2}	4.418×10^{-2}
G^*	6.091×10^{-3}	6.106×10^{-3}	2.490×10^{-2}	2.514×10^{-2}
υ^*	3.016×10^{-1}	2.992×10^{-1}	2.971×10^{-1}	2.875×10^{-1}

The reference analytical expressions for the 3D body centered cubic cell are (Sam *et al.*, 2017)

$$E^* = \frac{E}{V_C}\left[\frac{\left(\frac{12\sqrt{3}+9}{8\sqrt{3}+9}\right)(AL)^2+\left(\frac{192\sqrt{3}+768}{8\sqrt{3}+9}\right)(Al)}{AL+\left(\frac{64\sqrt{3}}{8\sqrt{3}+9}\right)\left(\frac{l}{L}\right)}\right], \tag{30}$$

$$G^* = \frac{E}{V_C}\left[\left(\frac{4\sqrt{3}}{9}\right)(AL) + \left(\frac{54+32\sqrt{3}}{9}\right)\left(\frac{l}{L}\right)\right] \tag{31}$$

$$\upsilon^* = \frac{\left(\frac{4\sqrt{3}}{8\sqrt{3}+9}\right)(AL)-\left(\frac{64\sqrt{3}}{8\sqrt{3}+9}\right)\left(\frac{l}{L}\right)}{AL+\left(\frac{64\sqrt{3}}{8\sqrt{3}+9}\right)\left(\frac{l}{L}\right)}. \tag{32}$$

We observe that the effective constitutive parameters obtained via NIAH using the cell configuration displayed in Fig. 5 do not coincide exactly with the reference value given by Sam *et al.* (2017). The difference of the reported values compared to the analytical ones is larger than in the 2D case and tends to increase for increasing cross section diameters.

Facing this and taking into consideration the insights gained in the analysis of the 2D problem, we use a 3D base cell configuration analogous to configuration III of the *body-centered square* cell. In other words, we generate a base cell defined only by perpendicular cuts to the axes of the elements. Figure 6 depicts a *body-centered cubic* structure with a base cell that satisfies that condition. The figure also shows different views of the base cell and gives details of the boundary conditions to be imposed, following the conventions described in the 2D case: blue nodes represent internal nodes, equally colored nodes define groups with the same boundary conditions (due to periodicity) and brown triangles stand for displacement constraints.

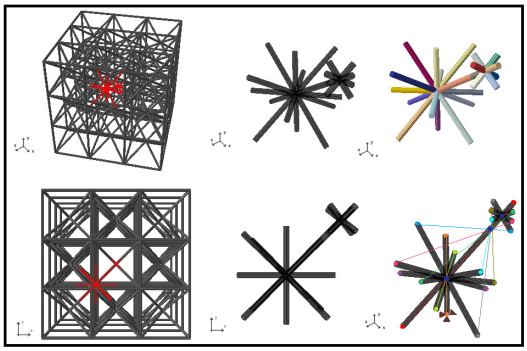

Figure 6. Alternative cell for the body-centered cubic structure: the cell is highlighted within the structure, different views of the cell are shown and the groups for boundary conditions are displayed.

The homogenized elastic tensors for this alternative configuration for the *body-centered cubic* cell are given in Table 6. The validation with the analytical values given by Sam *et al.* (2017) is given in Table 7.

Table 6. Homogenized elastic tensors for the alternative simple cubic base cell for different cross section diameters.

$\boldsymbol{E^H}(D=0.1)$	$\begin{bmatrix} 0.014021 & 0.005986 & 0.005986 & 0 & 0 & 0 \\ & 0.014021 & 0.005986 & 0 & 0 & 0 \\ & & 0.014021 & 0 & 0 & 0 \\ & & & 0.006106 & 0 & 0 \\ & sim & & & 0.006106 & 0 \\ & & & & & 0.006106 \end{bmatrix}$
$\boldsymbol{E^H}(D=0.2)$	$\begin{bmatrix} 0.057534 & 0.023217 & 0.023217 & 0 & 0 & 0 \\ & 0.057534 & 0.023217 & 0 & 0 & 0 \\ & & 0.057534 & 0 & 0 & 0 \\ & & & 0.025139 & 0 & 0 \\ & sim & & & 0.025139 & 0 \\ & & & & & 0.025139 \end{bmatrix}$

Table 7. Validation of constitutive parameters obtained in this work (NIAH) with the analytical values given by Sam et al. (2017) for the alternative body-centered cubic cell with $D = 0.1$ and $D = 0.2$.

Parâmetro Efetivo	NIAH	Sam *et al.* (2017)	NIAH	Sam *et al.* (2017)
	$D = 0.1$	$D = 0.1$	$D = 0.2$	$D = 0.2$
E^*	1.044×10^{-2}	1.044×10^{-2}	4.418×10^{-2}	4.418×10^{-2}
G^*	6.106×10^{-3}	6.106×10^{-3}	2.514×10^{-2}	2.514×10^{-2}
v^*	2.992×10^{-1}	2.992×10^{-1}	2.875×10^{-1}	2.875×10^{-1}

6. CONCLUSIONS

We presented a modified version of the NIAH, able to account for rotational degrees of freedom that occur in Euler-Bernoulli frame elements. This enables us to use NIAH to model cellular materials made of lattice-like base cells using frame rather than bar elements. In literature bar elements are often employed for these cases, but reliable results can only be ensured for stretch-dominated problems. With our proposed approach, both stretch-dominated and bending-dominated problems can be addressed, although this will be the matter of a forthcoming publication.

In this work we emphasize the modification made in the original NIAH method to handle frame elements and show how results are affected by the choice of the base cell (among different possibilities). We suggest a systematic procedure to define an adequate base cell, for which the homogenized elastic tensors and parameters coincide exactly with the analytical solution.

7. ACKNOWLEDGEMENTS

We would like to acknowledge State University of Santa Catarina – Udesc and the Graduate Program in Materials Science and Engineering – PGCEM for giving support in many levels, especially during the COVID pandemics. We also acknowledge the *Coordenação de Aperfeiçoamento de Pessoal de Nível Superior - CAPES* for the masters scholarship provided to the first author.

The first author also expresses special recognition to Sandmara Lanhi and to Kasem Theerakittayakorn for numerous e-mails discussing their previous publications which were fundamental for this research.

Finally, we thank *Fundação de Amparo à Pesquisa e Inovação do Estado de Santa Catarina (FAPESC)* for partial support through fundings number 2019TR779 and 2021TR843.

8. REFERENCES

Cheng, G.D., Cai, Y.W. and Xu, L, 2013, Novel implementation of homogenization method to predict effective properties of periodic materials. *Acta Mechanica Sinica*, Vol. 29, n. 4, pp. 550-556.

Guedes, J.M. and Kikuchi, N., 1990, Preprocessing and postprocessing for materials based on the homogenization method with adaptive finite element methods, *Computer Methods in Applied Mechanics and Engineering*, Vol. 83, pp.143-198.

Hassani, B. and Hinton, E., 1998, A review of homogenization and topology optimization I - Homogenization theory for media with periodic structure. *Computers and Structures* Vol. 69, pp.707-717

Jagiello, E. and Muñoz-Rojas, P. A., 2021. An extended multiscale finite element method (EMsFEM) analysis of periodic truss metamaterials (PTMM) designed by asymptotic homogenization, *Latin Amer. J. Solids Struct*. Vol. 18, n. 2, pp. e347.

Muñoz-Rojas, P.A., Carniel, T.A., Silva, E.C.N. and Öchsner, A., 2010, "Optimization of a unit periodic cell in lattice block materials aimed at thermo-mechanical applications", In Öchsner, A. and Murch, G.E. (eds.), *Heat Transfer in Multi-Phase Materials,* Adv. Struct Mater 2, Springer-Verlag Berlin Heidelberg.

Sam, P., Nanakorn, P., Theerakittayakorn, K. and Suttakul, P., 2017, Closed-form effective elastic constants of frame-like periodic cellular solids by a symbolic object-oriented finite element program, *International Journal of Mechanics and Materials in Design*, Vol. 13, pp. 363–383.

Sigmund, O., 1994, Materials with prescribed constitutive parameters: an inverse homogenization problem, *International Journal of Solids and Structures*, Vol. 31, pp. 2313–2329.

Weeks, J.S., 2022. *Mechanical Response of Lattice Structures under High Strain-Rate and Shock Loading*. Ph.D. Thesis, California Institute of Technology, Pasadena, California, USA.

Yan, J., Cheng, G., Liu, S. and Liu, L., 2006, Comparison of prediction on effective elastic property and shape optimization of truss material with periodic microstructure, *International Journal of Mechanical Sciences,* Vol. 10, pp.400-413.

Yang, Q.S. and Becker, W, 2004, Numerical investigation for stress, strain and energy homogenization of orthotropic composites with periodic microstructure and non-symmetric inclusions. *Computational Materials Science*, Vol. 31, pp. 169-180.

9. RESPONSIBILITY NOTICE

The authors are the only responsible for the printed material included in this paper.